Investigation on the Effect of Al on the Spinodal decomposition of Fe-Cr-Al system: A GPU Accelerated Phase-field method

Jepnghwan Lee, Kunok Chang *
Nuclear Engineering, Kyung Hee university, Republic of Korea
Corresponding author: kunok.chang@khu.ac.kr

1. Introduction

The development of accident tolerant fuel(ATF) cladding has been continuously studied [1,2]. Especially, ATF cladding has been focused on since the Fukushima accident in 2011 [3]. Although there are many candidates for ATF cladding materials, Fe-Cr-Al materials are considered ATF cladding materials due to excellent the corrosion and oxidation resistance at high temperature more than zirconium based cladding [4,5]. Also, as the Cr content increases, the oxidation and corrosion resistance are improved, however the α' phase, which give rise to embrittlement, is more easily formed. On the other hand, as the Al content increases, the mechanical properties is improved and suppress the formation of the α' phase, but the fabrication becomes difficult [6-8]. Therefore, it is important to find the optimal composition of Fe-Cr-Al.

Herein, we investigate quantitively the effect of Al concentration on microstructural evolution of Fe-Cr-Al system using phase field method and CALPHAD approach. In addition, the semi-implicit Fourier spectral method is well-known to solve the Cahn-Hilliard equation efficiently with high numerical stability, the compute unified device architecture(CUDA) is efficient to solve the Cahn-Hilliard equation. Therefore, to increase the computational efficiency, we apply the semi-implicit Fourier spectral method and parallel computing technique using compute unified device architecture(CUDA).

2. CALPHAD-based phase-field method and result

Herein, we simulate the spinodal decomposition using phase-field method and CALPHAD approach to evaluate quantitively the effect of Al in Fe-Cr-Al system.

2.1 Phase-field modeling in Fe-Cr-Al ternary system

We simulate the evolution of the Cr and Al concentration field by solving the following Cahn-Hilliard equation [9].

$$\frac{\partial c_{Cr}(r,t)}{\partial t} = V_m \nabla \cdot \left[M_{Cr,Cr} \nabla \frac{\delta F(r,t)}{\delta c_{cr}} + M_{Cr,Al} \nabla \frac{\delta F(r,t)}{\delta c_{Al}} \right]$$

$$\frac{\partial c_{Al}(r,t)}{\partial t} = V_m \nabla \cdot \left[M_{Al,Cr} \nabla \frac{\delta F(r,t)}{\delta c_{cr}} + M_{Al,Al} \nabla \frac{\delta F(r,t)}{\delta c_{Al}} \right]$$

where c_i is the concentration of i($=$ Cr, Al) component, respectively, and V_m is the moral volume, $M_{A,B}$ is the chemical mobility given by[10]

$$M_{Cr,Cr} = c_{Cr}[(1 - c_{Cr})^2 M_{Cr} + c_{Cr} c_{Al} M_{Al} + c_{Cr} c_{Fe} M_{Fe}]$$

$$M_{Al,Al} = c_{Al}[(1 - c_{Al})^2 M_{Al} + c_{Cr} c_{Al} M_{Cr} + c_{Al} c_{Fe} M_{Fe}]$$

$$M_{Cr,Al} = M_{Al} c_{Al} = c_{Cr} c_{Al} [c_{Fe} M_{Fe} - (1 - c_{Cr}) M_{Cr} - (1 - c_{Cr}) M_{Cr}]$$

where M_{Fe}, M_{Cr} and M_{Al} are the mobilities of the Fe,Cr and Al atom, respectively, and they are related Einstein's relation M = D/RT. Also, T is the absolute temperature and R is the gas constant, D_{Fe}, D_{Cr} and D_{Al} are the solute's diffusivity of Fe, Cr and Al atom.

The total free energy in Fe-Cr-Al ternary system is expressed by

$$F(r,t) = \int_V \left[f + \frac{1}{2}\kappa_{Fe} + \frac{1}{2}\kappa_{Cr} + \frac{1}{2}\kappa_{Al} \right] dV$$

where $f(c_{Fe}, c_{Cr}, c_{Al})$ is the chemical free energy in ternary system and κ_i is the gradient coefficient of Fe, Cr and Al. We assume that the gradient coefficient $\kappa_{Fe}, \kappa_{Cr}, \kappa_{Al}$ are same as

$$\kappa_C = \frac{1}{6}a_0^2 L_{FeCr}$$

where $a_0(= a_{Fe} + a_{Cr} + a_{Al})$ is the lattice parameter and L_{FeCr} is the regular solution interaction parameter.

2.2 Semi-implicit Fourier spectral method with a variable mobility

To improve the numerical stability, we apply the semi-implicit Fourier spectral method for solving the Cahn-Hilliard equation. In the Fourier, Eq. 1 is given by

$$\frac{\partial \tilde{c}_{Cr}(k,t)}{\partial t} = ik \cdot \left[M_{Cr,Cr} \left\{ ik'(\left\{\frac{\partial f}{\partial c_{Cr}}\right\}_{k'} + 2\kappa_C k'^2 \tilde{c}_{Cr} + \kappa_C k'^2 \tilde{c}_{Al}) \right\}_r + M_{Cr,Al} \left\{ ik'(\left\{\frac{\partial f}{\partial c_{Al}}\right\}_{k'} + 2\kappa_C k'^2 \tilde{c}_{Al} + \kappa_C k'^2 \tilde{c}_{Cr}) \right\}_r \right]_k$$

Where $k = (k_1, k_2)$ is the reciprocal vector in the Fourier space of magnitude k = $\sqrt{k_1^2 + k_2^2}$. The $\tilde{c}_i(k,t)$ and the $\left\{\frac{\partial f}{\partial c_i}\right\}_{k'}$ are the Fourier transforms of $c_i(r,t)$ and $\frac{\partial f}{\partial c_i}$ where i means concentration of Cr and Al, respectively. To improve the numerical stability, we applied semi-implicit Fourier spectral method. In the Eq. 6, the term $A\Delta t\kappa k^4 \tilde{c}_{Cr}^{n+1}$ is added to the left side and the term $A\Delta t\kappa k^4 \tilde{c}_{Cr}^n$ is added to the right side. Also, using by two term ($B\Delta t\kappa k^4 \tilde{c}_{Al}^{n+1}$, $B\Delta t\kappa k^4 \tilde{c}_{Al}^n$), we applied to same

method in the $\frac{\partial \tilde{c}_{Al}(k,t)}{\partial t}$. Therefore, the rearranged Eq. 6 is as follows.

$$\tilde{c}_{Cr}^{n+1} = \tilde{c}_{Cr}^{n} + \Delta tik \cdot \left[M_{Cr,Cr} \left\{ ik'(\left\{\frac{\partial f}{\partial c_{Cr}}\right\}_{k'}^{n} + 2\kappa_C k'^2 \tilde{c}_{Cr}^{n} + \kappa_C k'^2 \tilde{c}_{Al}^{n}) \right\}_r + M_{Cr,Al} \left\{ ik'(\left\{\frac{\partial f}{\partial c_{Al}}\right\}_{k'}^{n} + 2\kappa_C k'^2 \tilde{c}_{Al}^{n} + \kappa_C k'^2 \tilde{c}_{Cr}^{n}) \right\}_r \right]_k$$

2.3 CALPHAD-type free energy

The chemical free energy $f(c_{Fe}, c_{Cr}. c_{Al})$ in Eq. 3 is given by

$$f(c_{Fe}, c_{Cr}. c_{Al}) = c_{Fe}\overset{\circ}{G}_{Fe} + c_{Cr}\overset{\circ}{G}_{Cr} + c_{Al}\overset{\circ}{G}_{Al} + L_{FeCr}c_{Fe}c_{Cr} + L_{CrAl}c_{Cr}c_{Al} + L_{FeAl}c_{Fe}c_{Al} + RT \ln(c_{Fe} \ln(c_{Fe}) + c_{Cr} \ln(c_{Cr}) + c_{Al}\ln(c_{Al}))$$

where $\overset{\circ}{G}_{Fe}, \overset{\circ}{G}_{Cr}$ and $\overset{\circ}{G}_{Al}$ are the molar Gibbs free energies for pure elemental Fe, Cr and Al, respectively, L_{ij} is the interaction parameter between i and j composition, $R(= .3144/ \text{mol} \cdot K)$ is the gas constant, T is the absolute temperature, which is 710 K. There were calculated as follows [11,12]

$$\overset{\circ}{G}_{Fe} = +1225.7 + 124.134 \times T - 23.5143 \times T \times \ln(T) - 0.00439752 \times T^2 - 5.89269 \times 10^{-8} \times T^3 + 77358.5 \times T^{-1}$$

$$\overset{\circ}{G}_{Cr} = -8856.94 + 157.48 \times T - 26.908 \times T \times \ln(T) + 0.00189435 \times T^2 - 1.47721 \times 10^{-6} \times T^3 + 139250 \times T^{-1}$$

$$\overset{\circ}{G}_{Al} = -1193.24 + 128.245446 \times T - 38.5844 \times T \times \ln(T) + 0.018531982 \times T^2 - 5.764227 \times 10^{-6} \times T^3 + 74092 \times T^{-1}$$

$$L_{FeCr} = +20500 - 9.68T$$
$$L_{CrAl} = -54900 + 10.0T$$
$$L_{FeAl} = -122452.9 + 31.6455T$$

To increase the computational efficiency, we used dimensionless values. $r^* = r/l$, $\nabla^* = \partial/\partial(r/l)$, $t^* = tD/l^2$, $M^* = RT*M/D$, $f^* = (RT^*)$ and $\kappa^* = \kappa/(RT*l^*)$ with $D = D_{Al}$, $T^* = 875 K$ and l is a_0 value in Eq. 5. Also, the range of initial Cr concentration variation is [-0.005 - 0.005]. The non dimensionless time step value is 0.001, and the simulation size is the $512\Delta x \times 512\Delta y$ in 2D.

To investigate the effect of Al concentration on microstructural evolution of Fe-Cr-Al system, we simulated the 30 sets at 2D. We set the initial Cr concentration to 0.30, 0.35 and 0.40. Also, the initial Al concentration were set to 0.001, 0.003, 0.005, 0.007, 0.009, 0.01, 0.03, 0.05, 0.07 and 0.09 when for each Cr concentration in 2D simulation.

3. Simulation results and analysis

We analyzed the effects of Al using three way: the average α' phase precipitate area, the number of α' phase precipitates and the α' phase fraction over time, respectively.
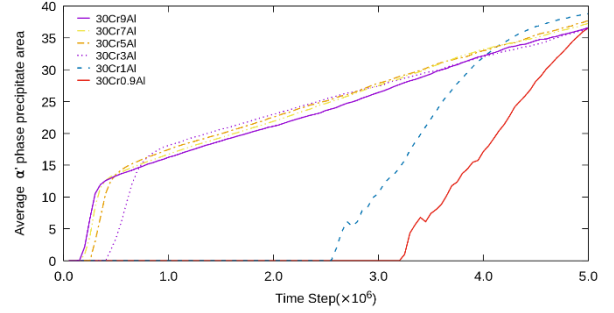

Fig 1. Plot of average α' precipitate area for Fe30Cr(0.1-9)Al

As shown in Fig. 1, when the Cr concentration was 30 *mol* %, the phase separation occurred early when the Al content was between 3 and 9 *mol* %, but it occurred relatively late when the Al content was 0.9 and 1 *mol* %. Also, when the Al content was between 0.1 and 0.7 *mol* %, the phase separation did not occur. In addition, the higher the Al concentration, the phase separation occurred early, the higher the number of α' precipitates as shown in Fig. 2 and the α' phase fraction was increased and it converged to 25 *mol* %.
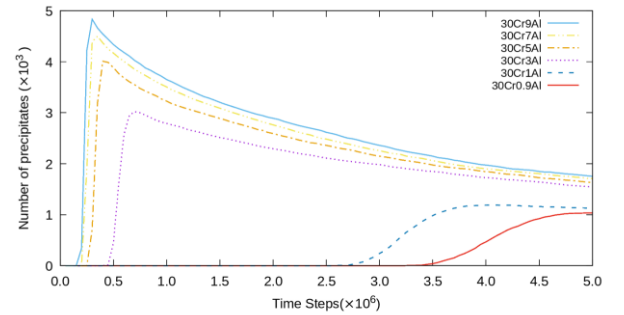

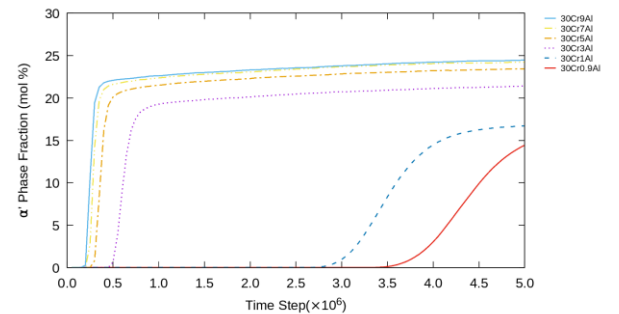Fig 2. Plot of the number of α' precipitates for Fe30Cr(0.1-9)Al

Fig 3. Plot of the α' phase fraction for Fe30Cr(0.1-9)Al
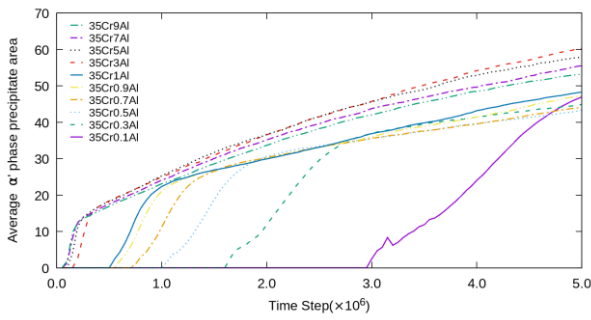
Fig 4. Plot of average α' precipitate area for Fe35Cr(0.1-9)Al

Similarly, when the Cr concentration was 35 *mol* %., as Al concentration increased, phase separation occurred early as shown in Fig. 4 and the incubation time for nucleation is longer. However, unlike when the Al concentration was 3 *mol* % or more, phase separation occurred relatively early, it was less than 1 *mol* %, the start time interval of phase separation was relatively longer.
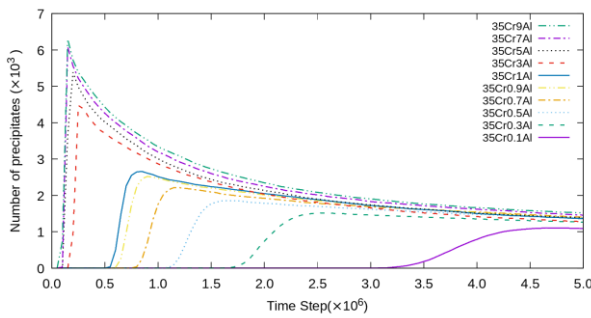

Figure 5. Plot of the number of α' precipitates for Fe30Cr(0.1-9)Al

In the early stage, the number of α' phase precipitates was higher than that of less than 1 *mol* % when the Al concentration was more than 3 *mol* %. Also, the phase fraction converged to 30 *mol* %. As the 30 *mol* % Cr concentration, the α' phase fraction increases when the Al concentration increases as shown Fig. 6. In addition, to verify to this trend, we calculated the α' phase fraction using Factsage software. As shown Fig. 7, the α' phase fraction was higher as Al concentration increased.
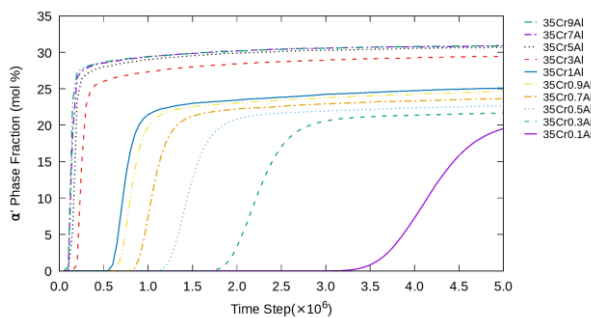

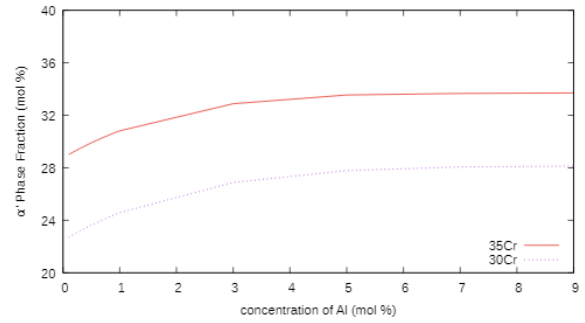Fig 6. Plot of average α' precipitate area for Fe35Cr(0.1-9)Al

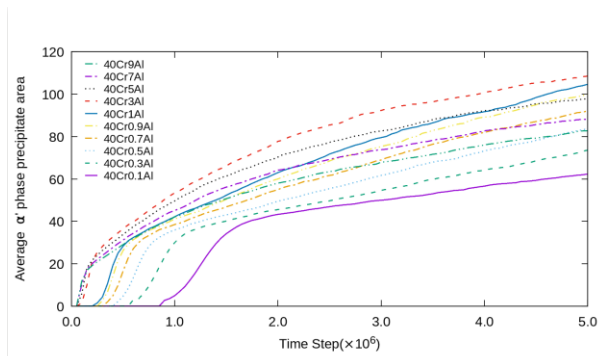Fig 7. Plot of the α' phase fraction using Factsage software

Fig 8. Plot of average α' precipitate area for Fe40Cr(0.1-9)Al

As shown Fig. 8, the phase separation when the Cr concentration was 40 *mol* % occurred early in comparison with Cr concentration of 30 *mol* % and 35 *mol* %. Also, the start time interval of phase separation was relatively short. As shown Fig. 9, the phase fraction converged to 36 *mol* %.
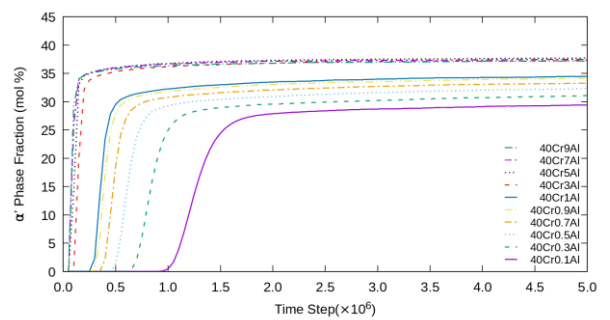

Fig 9. Plot of average α' precipitate area for Fe35Cr(0.1-9)Al

3. Conclusions

As the Al concentration increases, phase separation occurs early, and phase fraction increases. Also, phase fraction converges at certain Al content.

REFERENCES

[1] R. L. Klueh, D. R. Harries, High-chromium ferritic and martensitic steels for nuclear applications, AsTM West Conshohocken, PA, 2001.

[2] R. Klueh, A. T. Nelson, Ferritic/martensitic steels for next-generation reactors, Journal of Nuclear Materials 371 (1-3) (2007) 37–52.

[3] S. J. Zinkle, G. Was, Materials challenges in nuclear energy, Acta Materialia 61 (3) (2013) 735–758.

[4] B. A. Pint, K. A. Terrani, M. P. Brady, T. Cheng, J. R. Keiser, High temperature oxidation of fuelcladding candidate materials in steam–hydrogen environments, Journal of nuclear materials 440 (1-3)(2013) 420–427.

[5] K. A. Terrani, S. J. Zinkle, L. L. Snead, Advanced oxidation-resistant iron-based alloys for lwr fuelcladding, Journal of Nuclear Materials 448 (1-3) (2014) 420–435.

[6] P. Grobner, The 885 f (475 c) embrittlement of ferritic stainless steels, Metallurgical Transactions 4 (1)(1973) 251–260.

[7] D. Chandra, L. Schwartz, Mössbauer effect study of the 475‡ c decomposition of fe-cr, MetallurgicalTransactions 2 (2) (1971) 511–519.

[8] H. Solomon, L. M. Levinson, Mössbauer effect study of'475 c embrittlement'of duplex and ferriticstainless steels, Acta Metallurgica 26 (3) (1978) 429–442.

[9] J. W. Cahn, On spinodal decomposition, Acta metallurgica 9 (9) (1961) 795–801

[10]日本金属学会,金属データブック,丸善(1974) 81–83

[11] A. Dinsdale, Sgte data for pure elements, calphad 15 (4) (1991) 317–425

[12] M. Jacobs, R. Schmid-Fetzer, T. Markus, V. Motalov, G. Borchardt, K.-H. Spitzer, Thermodynamicsand diffusion in ternary fe–al–cr alloys, part i: Thermodynamic modeling, Intermetallics 16 (8) (2008)995–1005